Earth and Planetary Science Letters 452 (2016) 171–177

Contents lists available at ScienceDirect

Earth and Planetary Science Letters

www.elsevier.com/locate/epsl

# West–east transition from underplating to steep subduction in the India–Tibet collision zone revealed by receiver-function profiles

Danian Shi [a,*], Wenjin Zhao [b], Simon L. Klemperer [c], Zhenhan Wu [b], James Mechie [d], Jianyu Shi [a], Guangqi Xue [a], Heping Su [a]

[a] MLR Key Laboratory of Metallogeny and Mineral Assessment, Institute of Mineral Resources, CAGS, 26 Baiwanzhuang Road, Beijing 100037, China
[b] Chinese Academy of Geological Sciences, 26 Baiwanzhuang Road, Beijing 100037, China
[c] Department of Geophysics, Stanford University, Stanford, CA 94305-2215, USA
[d] Deutsches GeoForschungsZentrum - GFZ, Section "Geophysical Deep Sounding", Telegrafenberg, D-14473 Potsdam, Germany

ARTICLE INFO

*Article history:*
Received 18 February 2016
Received in revised form 21 July 2016
Accepted 27 July 2016
Available online xxxx
Editor: P. Shearer

*Keywords:*
continental collision
crustal and upper-mantle structure
receiver-function imaging
Tibetan plateau
continental subduction
lower-crustal delamination

ABSTRACT

Closely-spaced receiver-function profiles in the east-central India–Tibet collision zone reveal drastic west–east changes of the crustal and upper mantle structure. West of ~91.5°E, we show the Indian crust-mantle boundary (Moho) extending subhorizontally from ~50 km depth below sea level under the High Himalaya to ~90 km under the central Lhasa terrane. Further north, this boundary transitions to become the top of the Indian lithospheric mantle and, becoming faint but still observable, it can be tracked continuously to ~135 km depth near ~31.5°N. The top of the Indian lithospheric mantle is clearly beneath the Tibetan Moho that is also a conspicuous boundary, undulatory at 60–75 km depth from the central Lhasa terrane to the north end of our profile at ~34°N. This geometry is consistent with underthrusting of Indian lower crust and underplating of the Indian plate directly beneath southern Tibet. In contrast, east of ~91.5°E, the Indian Moho is only seen under the southernmost margin of the Tibetan plateau, and eludes imaging from ~50 km south of the Yarlung-Zangbo suture to the north. The Indian lower crust thins greatly and in places lacks a clear Moho. This is in contrast to our observation west of ~91.5°E, that the Indian lower crust thickens northwards. A clear depression of the top of the Indian lower crust is also observed along west–east oriented profiles, centered above the region where the Indian Moho is not imaged. Our observations suggest that roll-back of the Indian lithospheric mantle has occurred east of ~91.5°E, likely due to delamination associated with density instabilities in eclogitized Indian lower crust, with the center of foundering beneath the southern Lhasa terrane slightly east of 91.5°E.



## 1. Introduction

The Tibetan Plateau is the spectacular consequence of the ongoing India–Eurasia continental collision beginning at ~57 Ma (e.g., Argand, 1924; Tapponnier et al., 2001; Leech et al., 2005). The post-collisional convergence between the two continents likely exceeds 2000 km (Dupont-Nivet et al., 2010). Previous studies suggest that this convergence has been accommodated in part by underthrusting of Indian lower crust beneath the Himalaya (Zhao et al., 1993; Schulte-Pelkum et al., 2005) and for at least 150 km north of the Yarlung Zangbo Suture (YZS) to at least ~31°N between longitudes 85°E and 92°E (Kind et al., 2002; Nábělek et al., 2009; Shi et al., 2015). However, this amount of underplating can only account for the convergence during the last 10 Ma, given the modern underthrusting rate of 1.6 cm/yr of Indian lower crust under southern Tibet (Wang et al., 2001). How the Indian lower crust was accommodated before this time remains largely speculative. The underplating interpretation of Nábělek et al. (2009) suggests the Indian lithospheric mantle remains attached to the sub-horizontal Indian lower crust to ~31°N at ~85°E. In contrast, Kosarev et al. (1999) and Shi et al. (2015) show the Indian lithospheric mantle detaching from the crust ~50 km north of the surface trace of the YZS at ~90°E, and ~50 km south of the surface trace of the YZS at ~92°E, implying steep subduction may also play an important role in accommodating the vast amount of convergence. How and why the Indian lithospheric mantle transitions from almost horizontal underplating to steep subduction

* Corresponding author. Fax: +86 10 68327263.
*E-mail addresses:* shidanian@cags.ac.cn (D. Shi), zhaowj@cae.cn (W. Zhao), sklemp@stanford.edu (S.L. Klemperer), wuzhenhan@sohu.com (Z. Wu), jimmy@gfz-potsdam.de (J. Mechie), shi5945@sina.cn (J. Shi), xueguangqi@cags.ac.cn (G. Xue), suheping1950@163.com (H. Su).

http://dx.doi.org/10.1016/j.epsl.2016.07.051
0012-821X/

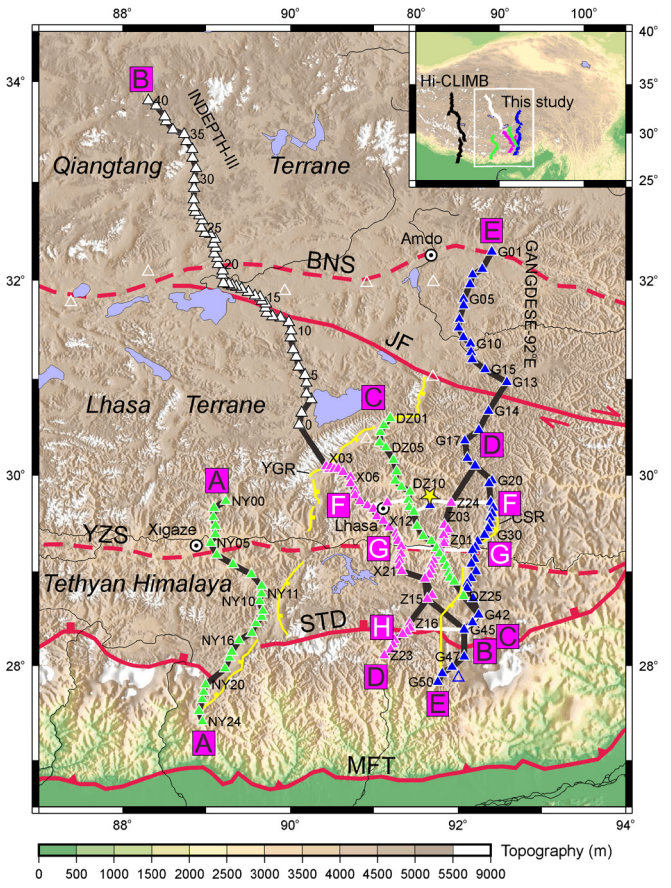


**Fig. 1.** Gangdese and INDEPTH III seismometer locations superimposed on the topography, east-central India–Tibet collision zone. Blue, pink and green triangles: Gangdese seismic stations deployed in 2011 (Gangdese 92°E: Shi et al., 2015), 2012 and 2014; white triangles: INDEPTH III seismic stations (Kind et al., 2002; Tilmann et al., 2003; Shi et al., 2004). (Open triangles were not used in constructing images in Fig. 2.) Black and white lines connect stations used to form profiles A, B, C, D, E, F, G and H. Dashed red lines mark the Yarlung Zangbo (YZS) and Banggong–Nujiang (BNS) sutures. Red lines delineate the Main Frontal Thrust (MFT), South Tibet Detachment (STD) and the dextral Jiali fault (JF). Yellow lines show bounding faults of the Yadong–Gulu (YGR) and the Cona–Sangri rift systems (CSR) (after Taylor and Yin, 2009). Yellow star symbol indicates a major center of ~18–12 Ma porphyry deposits. Inset shows the extent of this map (white rectangle) and the Hi-CLIMB main-profile seismic stations (black triangles) on the topographic map of the Tibetan plateau.

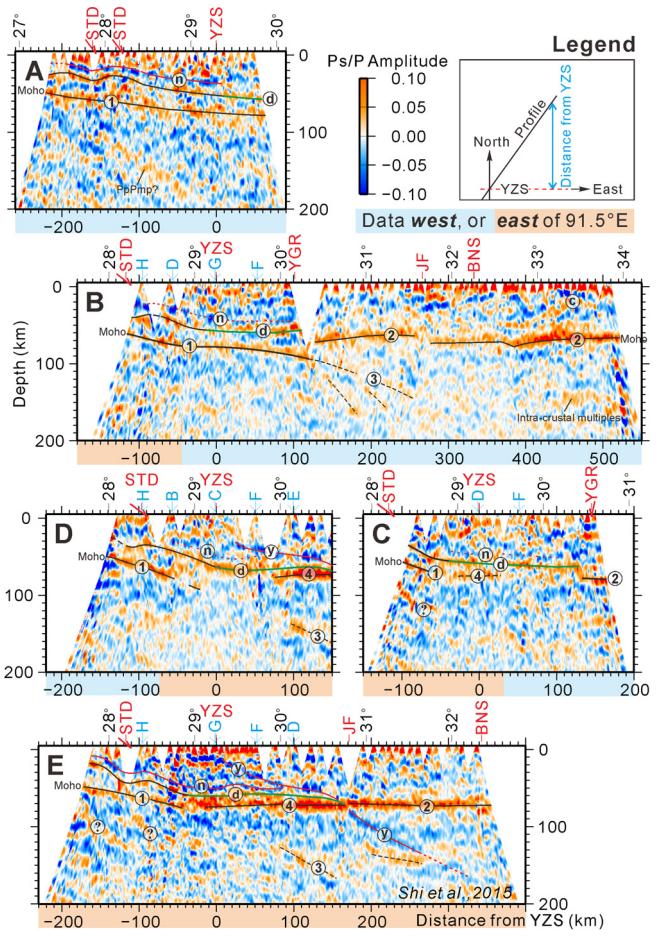


**Fig. 2.** Seismic images and interpretations of crustal and upper-mantle structure along five closely-spaced, near south-to-north trending profiles showing abrupt west-to-east change in the east-central India–Tibet collision zone. The same images without interpretive lines are shown in Fig. S2. All images are constructed with P-receiver functions, using a fixed horizontal stacking bin width of 3.5 km. Horizontal distances are relative to 29.25°N (latitude of YZS), and depths are relative to sea level. Positive and negative amplitudes are plotted in red and blue, respectively marking interfaces with increasing and decreasing impedance with depth. Interfaces are shown by solid lines when the conversions are strong, and by dashed lines when the conversions are weak or less confidently interpreted. '1', '2' and '4' indicate the conversions from the crust-mantle boundary (or Moho). 'd' denotes the doublet conversion from the top of the Indian lower crust, 'n' the negative conversion tracking above the doublet conversion, '3' the top of Indian lithospheric mantle, 'y' the Yarlung Zangbo converter (Shi et al., 2015). The crossing points of each profile with other profiles are marked above the profiles.

remains uncertain. Here we present new evidence for the rapid spatial transition between these two modes of convergence.

## 2. Data and method

Between September of 2011 and September of 2012, we deployed our Gangdese-92°E seismic array in southern Tibet. The results from this deployment suggest a steep subduction of the Indian plate in the east-central India–Tibet collision zone (Shi et al., 2015). In order to further clarify Tibet's deep structure, especially how the Indian plate transitions from underplating to steep subduction, we deployed four shorter linear seismic arrays from 2012–2014 (Fig. 1) in the area previously best studied by the INDEPTH II and III arrays (1994 and 1998–1999) (Kosarev et al., 1999; Kind et al., 2002; Tilmann et al., 2003; Shi et al., 2004) and the Gangdese-92°E array. All our new arrays were equipped with Guralp 3ESPCD broadband seismometers, and operated for 12 months. Wherever possible we deployed our new seismic arrays outside of the north–south trending rift systems (Fig. 1) in order to focus on the collisional structure between the two continents. Profiles (Figs. 2 and 3) combining the data acquired by our new arrays and those from the INDEPTH III and Gangdese-92°E experiments, all together comprising 198 seismometer locations, provide us with a better view of the east-central India–Tibet collision zone, from the High Himalaya, across the YZS, to the Banggong–Nujiang Suture (BNS) and central Tibet.

We obtained images of the crustal and upper-mantle structure of the east-central India–Tibet collision zone using common conversion point (CCP) stacks of P receiver functions (PRFs), a well-established method which has been applied in many similar studies of the Tibetan plateau (e.g. Kosarev et al., 1999; Kind et al., 2002; Nábělek et al., 2009; Zhao et al., 2011). This method enhances S waves converted from P waves of distant earthquakes that impinge on seismic interfaces. It detects interfaces and describes their properties based on the time delays between the direct and converted waves that are mainly proportional to the depths of the interfaces, and on the amplitudes of the converted waves that depend on the magnitudes and signs of the velocity contrasts.

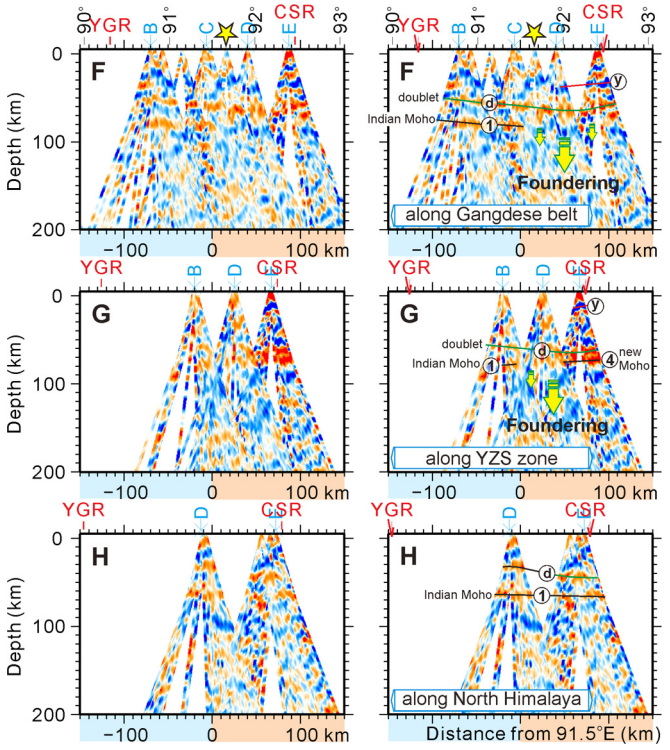


**Fig. 3.** Seismic images (left) and interpretations (right) of crustal and upper-mantle structure along three west-to-east trending profiles showing abrupt change at ~91.5°E in the east-central India–Tibet collision zone. All the images are constructed and annotated as for Fig. 2, but the horizontal distances are relative to 91.5°E (longitude of presumed transition boundary). Indian Moho (marked '1') is present under the southern margin of Tibet (~90 km south of the YZS) along the entire profile H, but eludes imaging to the east of ~91.5°E along the two northern profiles F and G, accompanied by a subsidence of the top of the Indian lower crust (delineated by converter 'd'). We attribute all these features to a roll-back of Indian mantle lithosphere east of ~91.5°E, and a foundering of Indian lower crust between the Yadong–Gulu (YGR) and the Cona–Sangri rifts (CSR).

We used teleseismic events with magnitudes ≥5.5 and epicentral distances between 30° and 90°. To ensure that only good-quality waveforms were used, we also applied a visual selection process to all the data. After all these processes, we obtained 1978, 4746, 2344, 2308, 4112, 1009, 722, and 606 RFs for the profiles A, B, C, D, E, F, G and H respectively, averaging about 76 RFs per station. We performed time-domain iterative deconvolution (Ligorria and Ammon, 1999) in the calculation of the RFs, in which the Gaussian filter factor was set to 2 to retain sufficiently high frequencies (from ~0.02 Hz up to ~1 Hz) to image crustal and upper-mantle structure. We isolated the converted from the incident waves using the wave-vector method (Reading et al., 2003), which decomposes P- and S-waves and removes the effect of the free surface by multiplying the inverse matrix of free-surface response with the observed vertical, radial and transverse components of the data. A free-surface response matrix, calculated for surface velocities of Vp = 5.31 km/s and Vs = 2.98 km/s, removed most of the effects of the free surface. All the RFs were migrated from time to space in a 3-D volume by tracing the rays from the location of each seismic station through a layered reference model (Supplementary Table S1). Unless otherwise stated, all the RFs were finally projected due west or due east onto the profiles for the nearly south-to-north oriented profiles (lines A–E), and projected due south or due north onto the profiles for the nearly west-to-east oriented profiles (lines F–H), and stacked onto cross-sections formed along each profile, no matter how large the obliquity of any particular profile to true north or to true east (profile B trends ~330°, profile D ~030°). Projection due west or due east is parallel to both the surface geological trends and most deep-seated structures (see Figs. 1, S3, S4 and S5) in the study region, so that our images along south-to-north oriented profiles should show the true dips of north-dipping structures. Because of the relatively steep dips we are imaging, we use dip-moveout ('DMO') to ensure proper imaging (Figs. S3, S4, S5). Because converters within the mantle typically have very low amplitudes, we only interpret those features on our migrated images (Figs. 2 and 3) that are coherent on DMO plots and that can be correlated or confirmed on adjacent profiles.

## 3. Results and interpretations

Our closely-spaced profiles show the crustal and upper-mantle structure of the east-central India–Tibet collision zone very clearly, but with surprisingly big differences between the nearly south-to-north oriented profiles (Figs. 2, 4, S2), and clear west-to-east changes at ~91.5°E on the west-to-east oriented profiles (Fig. 3).

West of ~91.5°E, the Indian Moho (marked '1' in Figs. 2, 3 and 4) extends smoothly northwards from a depth of ~50 km under the High Himalaya, across the YZS, to the southern Lhasa terrane (all depths are given below sea-level; surface elevation of ~5 km on the Tibetan Plateau must be added to Moho depths to give crustal thickness). The Indian Moho is clearly imaged to ~90 km depth at ~30.3°N along profile B. In contrast, east of ~91.5°E, the Indian Moho (Figs. 2 and 3) is only seen over a short distance under the southern margin of the plateau, from ~50 km depth under the High Himalaya to ~80 km depth, ~60 km south of the YZS, and then it eludes imaging further to the north. In addition to the sharp change at ~91.5°E, we also observe some small but marked variations of Moho dip under the High Himalaya, from ~8° on the westernmost profile A (Fig. 2A), to ~17.5° on profile D (Figs. 2D, S5), and then to ~7° on the easternmost profile E (Fig. 2E; Shi et al., 2015). The steepest Indian Moho we observe (on profile D) is slightly west of, but close to, 91.5°E.

Unlike the Indian Moho, the Tibetan Moho (marked '2' in Figs. 2B, E) is either horizontal or deepens slightly to the south, and is clearly separated vertically above the top of the Indian lithospheric mantle (ILM) that we will address below. Along profile B, '2' is strong and shallows northwards from ~70 km to ~60 km south of the JF, but becomes weaker and deeper, ~70 km depth, between the JF and the Banggong–Nujiang suture (BNS). The Tibetan Moho becomes strong again north of the BNS with the southern margin of this segment depressed towards the south.

At mantle depths, we also observe some positive north-dipping conversions (marked '3', '?' and 'PpPmp?' in Fig. 2). 'PpPmp?' and '?' are possible crustal and intra-crustal multiples (see Fig. S6), because they dip north, the same direction as the overlying Moho and intra-crustal structure. But north-dipping converters marked '3' cannot be simple multiples because the overlying Moho and intra-crustal structures are flat or dip south. These conversions are similar to those previously observed along the Hi-CLIMB profile at 85°E, and interpreted by Nábělek et al. (2009) as related to diffuse deformation within the ILM. In our images, '3' project downwards, albeit discontinuously, from the northern end of the Indian Moho on three different profiles (Figs. 2B, D, E). Along profile B, conversion '3' can be traced from ~90 km at the northern limit of the Indian Moho to ~135 km depth beneath the Jiali fault (JF), with its dip increasing from ~8° to ~20° (Fig. S4). We interpret this conversion '3' to be the top of the Indian lithospheric mantle (ILM), beneath Tibetan mantle, and suggest the resulting smaller impedance change makes converter '3' (mantle over mantle) weaker than '1' (crust over mantle) (Fig. 4b). Conversion '3' is close to the location where Kosarev et al. (1999) previously interpreted the top of the ILM, and is sub-parallel to the Indian lithosphere-asthenosphere boundary (I-LAB) imaged by

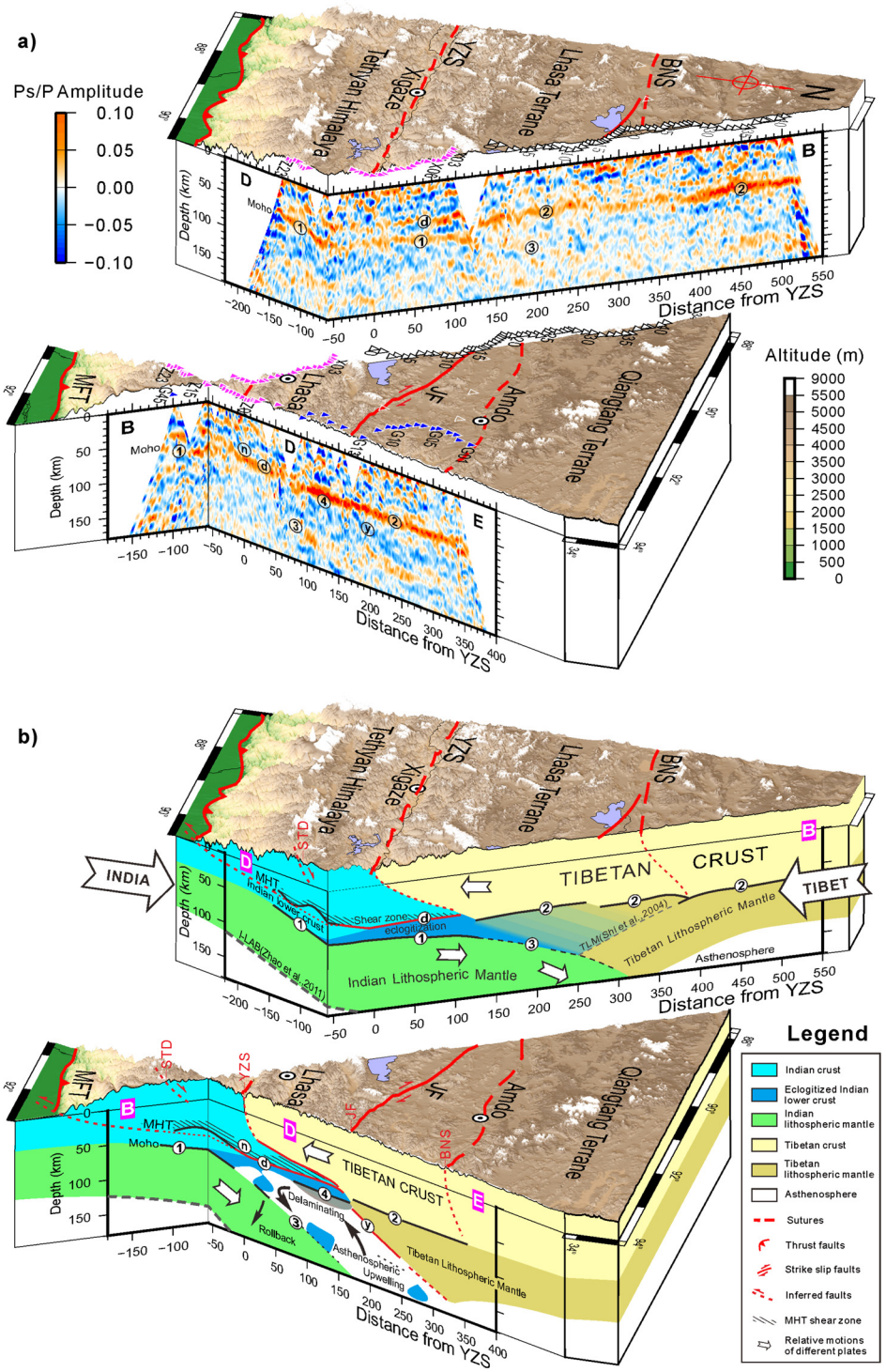


**Fig. 4.** Three-dimensional view of observed (a) and interpretive (b) cross-sections B and D concatenated with the northern part of profile E, with viewing azimuth towards N105°W and elevation angle down 30°. India-Asia convergence is currently accommodated by underplating of Indian lower crust and lithospheric mantle along profiles A and B to the west of ~91.5°E, but by foundering of Indian lower crust and steep subduction of Indian lithospheric mantle along profiles D and E. The undulating portions of converter 'd' are interpreted as thrust growing above the MHT to form ramp-and-flat structures (Fig. S7). Diagonal ruling shows the accumulated shear zones of the MHT, characterized by a low-velocity region between converters 'n' and 'd'. The eclogitized Indian lower crust is shown in dark blue, mainly beneath the horizontal portion of converter 'd'. The triangular area with colors transitioning from blue to khaki in the top panel of Fig. 4b denotes the Tibetan lithospheric mantle contaminated by materials scraped from the underplating Indian plate. Dashed grey lines mark the Indian lithosphere-asthenosphere boundary (I-LAB) (Zhao et al., 2011) and the top of the Tibetan lithospheric mantle (TLM) (Shi et al., 2004) obtained on the INDEPTH profiles. Other annotation as in Figs. 1 and 2.

Zhao et al. (2011) (see Shi et al., 2015). Our interpretation is also consistent with P-wave arrival-time tomography showing subduction of the Indian lithospheric mantle at moderate angle beneath the Himalaya in our study region (Li et al., 2008). Along profiles D and E, the conversions '3' are even weaker and further separated from the northern edge of the Indian Moho. We interpret them as the top of the ILM as on Profile B, and speculate that their presence north of 30°N relates to a local velocity decrease atop the ILM, and their absence further south is due to the lack of impedance contrast there.

Our older results showed marked southeast-dipping conversions on the northern end of Profile B (INDEPTH-III), from the Moho at ~32.7°N, north of the BNS, down to ~135 km depth beneath the JF (Shi et al., 2004). However, on our current image (Fig. 2B), there are only faint and diffuse patches of south-dipping energy when the seismic data are projected, as here, onto a north–south line (cf. Shi et al., 2004). This change of appearance with orientation can be explained by southeastward (rather than southward) subduction of the TLM along the BNS. Profile B also shows faint north-dipping positive converters beneath conversion '3' (dashed black lines without labels in Fig. 2B) (cf. Shi et al., 2004), possibly all representing deformation structures resulting from interaction between the ILM and the TLM beneath the JF.

The negative-polarity (seismic wavespeed decreases downwards) Yarlung-Zangbo converter (YZC), which was clearly imaged on the 92°E profile (profile E, Fig. 2E) and interpreted as a manifestation of the YZS in the crust and the top of an asthenospheric wedge in the mantle (Shi et al., 2015), can be partly seen on profile D (marked 'y' in Fig. 2D, and also Fig. 3, profiles F and G) but is not visible on profile B. Based on the crustal and upper-mantle structure resolved by our west–east profiles (Figs. 3F, G), we infer that an asthenospheric mantle wedge exists under profile D north of the YZS, and ascribe the lack of negative conversions in the mantle on profile B to the lack of, or closure of, an asthenospheric mantle wedge there. Similarly, the absence on profile B of a crustal converter analogous to the YZC on profiles D and E may suggest faulting on the YZS is less active along profile B than further east, or that the YZS has been inactive since 23 or 18.3 Ma (Yin et al., 1994) and then obscured by post-collisional magmatism that continues to more recent times younger in the west (profile B) than in the east (profile D) (Zhang et al., 2014).

The most prominent feature in the crust is the positive converter marked 'd' (Figs. 2 and 3), which can be seen on all the profiles. It lies 20–25 km above the Indian Moho on profile B in the region of the YZS, and is equivalent to the doublet phase observed on the INDEPTH and Hi-CLIMB profiles (Kind et al., 2002; Nábělek et al., 2009). We interpret 'd' as continuing upwards to the south in a ramp-flat-ramp geometry, with an average dip of ~15°, but locally as steep as 40°. Additionally, a negative interface (marked 'n' in Fig. 2) can be seen clearly on profiles A and E, but diffusely on profiles B, C and D, apparently tracking the positive interface 'd'. This negative-over-positive pair of interfaces as should represent top and bottom of a low-velocity zone.

The undulation of converter 'd' is clearly imaged on profile A, under the High Himalaya and immediately north of the South Tibet Detachment (STD) (Fig. 2A). However, only the northern ramp is fully imaged by all our near south-north profiles, with depths deepening clearly from west to east from profile A, to profile D, and then to profiles B and E (Fig. 2). Analogous ramp-flat-ramp geometry of the MHT has been seismically imaged in the western Himalaya (Caldwell et al., 2013; Gao et al., 2016). A geodetically-constrained inversion of denudation data at 90°E in western Bhutan near our study region has argued for a ramp as steep as 40° immediately north of the STD (Le Roux-Mallouf et al., 2015) implying that our imaged dip of up to 40° is not unreasonable. A recent near-vertical incidence seismic-reflection profile at 81°E resolves a ramp north of the STD that dips ~19° north to ~60 km depth (Gao et al., 2016). Gao et al. (2016) suggest this active ramp of the MHT underlies a thick duplex (up to 30 km thick) of thrust slices of Indian middle crust bounded by former traces of the MHT. According to their results, our observation of the ramp-flat-ramp geometry can also be interpreted as resulting from sequential thrusting on or close to the MHT (see Fig. S7). In this scenario, the undulating portion of converter 'd' represents the top of Indian lower crust, or the base of an earlier shear zone of the MHT while the converter 'n' represents the top of the duplex of Indian middle crust and an older MHT shear zone. The current faulting on the MHT may reside fully inside the Indian lower crust. The lack of an impedance contrast across it and the small width of the fault zone may prevent it from being imaged by receiver functions at lower frequencies (see Fig. S7), but not from being imaged by the Gao et al. (2016) reflection profile at higher frequencies.

The sub-horizontal portion of converter 'd' (colored green in Figs. 2 and 3) continues north to ~30.3°N, roughly tracking the Moho on profile B. On profiles D and E, this portion of 'd' is also horizontal north of the YZS and can be traced to the vicinity of the Jiali fault at ~30.8°N. An intriguing distinction between the profiles B and D is that on profile D we cannot recognize a separate Moho, or base to the doublet, for ~50 km north of the YZS (Fig. 2D). This absence of a Moho converter is clearly confirmed on the west–east oriented profiles (Figs. 3F, G). On all our profiles we interpret 'd' as the top of Indian lower crust, but the Indian lower crust may have already, at least partly, transitioned through the metamorphic phase-change boundary of eclogitization (Hetényi et al., 2007) in its northern sub-horizontal portion (see Fig. 4b). The Indian lower-crustal doublet is similar thickness or somewhat thicker along profile B (20 km) than further west – 15–20 km observed at ~85°E (Nábělek et al., 2009; Wittlinger et al., 2009) and northwest of Lhasa (Kind et al., 2002). The ~20 km-thick Indian lower crust is also present under nearby profile A, along ~89°E, although the Indian Moho appears more complicated along this profile. However, the lower-crustal doublet along profiles A and B is significantly thicker than to the east, where the Indian lower crust thins to 10–15 km along profile E at ~92°E (Fig. 2E; Shi et al., 2015) and ~10 km at 93–94°E (Zurek, 2008), above the presumed asthenospheric mantle wedge east of ~91.5°E.

Along west–east profiles, we observe a smooth variation of the depth of converter 'd' (Figs. 3F, G). On profile F, from west to east, the depth of converter 'd' changes from ~52 km beneath profile B, to ~62 km beneath profile D, then to ~55 km beneath profile E. On profile G, the depth changes from ~55 km beneath profile B to ~65 km beneath profile E. These observations suggest that a depression of the top of the Indian lower crust is present in our study region, with a center approximately where the Indian Moho does not produce a conversion.

We infer that east of ~91.5°E in our study region, Indian lower crust has been thinned by delamination of density instabilities due to the widely inferred eclogitization (Kind et al., 2002; Schulte-Pelkum et al., 2005; Hetényi et al., 2007; Nábělek et al., 2009; Wittlinger et al., 2009; Shi et al., 2015) above a subducting Indian slab that is rolling back. We attribute the depression of converter 'd' (Fig. 3) to foundering of Indian lower crust, the absence of a Moho converter above the mantle wedge along profile D to direct contact of the Indian lower crust with asthenosphere (Fig. 4b), and we infer the brightening northwards again of this converter above the wedge along profiles D and E ('4' in Fig. 2) marks a thin mantle lid formed from the cooling of asthenospheric material. We observe some similar conversions along profile C ('4' in Fig. 2C). As the corresponding portion of profile C is located between profiles D and E (Fig. 1), we interpret these conversions along profile C to correspond to a newly formed thin mantle lid as for profiles D and E. The steeper Moho observed along profile D under the High Himalaya may also be associated with the roll-back of Indian lithospheric mantle, although it resides a little west of the ~91.5°E transition boundary.

## 4. Discussion and conclusions

Recent body-wave tomography has found low velocities beneath the Yadong–Gulu rift system (YGR) at ~90.5°E and the Cona–Sangri rift system (CSR) at ~92°E, interpreted as astheno-

spheric upwelling due to lithospheric delamination beneath the rift (Ren and Shen, 2008) or upwelling around a fragmenting subducting Indian slab (Liang et al., 2012, 2016). However, our seismic images, that have higher resolution than the tomography, show that thinner Indian lower crust is clearly observed away from these two rift systems, and thus thinning of the Indian lower crust can not be accounted for only by erosion of upwelling asthenosphere associated with the formation of these rift systems. Nor can lower-crustal erosion by asthenosphere account for the steeper Indian subduction observed along profile D than along profiles B and E.

The cratonic Indian lithosphere (crust and mantle) is thought to be less dense than the underlying mantle so that Indian lithosphere may underplate horizontally immediately beneath the crust of the overlying plate (Argand, 1924) after the break-off of the Indian oceanic slab at ~45 Ma (Powell and Conaghan, 1973) or at ~30 Ma (DeCelles et al., 2002). Both our profiles A and B and the HiCLIMB profile (Nábělek et al., 2009) are consistent with the underplating model. However, after removal of the Indian upper crust, and part or all of the Indian lower crust, the remaining Indian lithosphere is denser than the deeper upper mantle, and lithospheric subduction is favored (Capitanio et al., 2010). Our profiles D and E are consistent with roll-back and steeper subduction of the Indian lithospheric mantle. The transition from underplating to steeper subduction occurs at ~91.5°E. The transition may be explained, on a larger scale, by eastward subduction and westward retreat of the Burmese arc during clockwise rotation of the Sunda block (e.g. Li et al., 2008; Russo, 2012). The thinned Indian lower crust directly above the asthenospheric mantle wedge suggests that this transition may have a causal link to the thinning of Indian lower crust. Taking all our observations together, we conjecture that the transition from underplating to steeper subduction may be due to the dense, eclogitized Indian lower crust counteracting the buoyancy of the underlying Indian lithosphere. The upwelling of asthenosphere and roll-back of the Indian lithospheric mantle may result from eclogitization-induced foundering of parts of the Indian lower crust triggered by density instabilities along the collision zone (Fig. 4b). The depression of the top of Indian lower crust along profiles F and G and the steeper Indian Moho observed along profile D than along profiles A, B and E probably suggests a local foundering center of the Indian lower crust somewhere around 18–12 Ma where intensive magmatism and metallogenesis (Hou and Cook, 2009) has been observed (yellow star symbols in Figs. 1, 3). However, we do not know whether the system is recovering from a former episode of roll-back or developing a new roll-back of Indian lithospheric mantle.

We recognize at least two possible causes for foundering of Indian lithospheric material. Delamination *sensu stricto*, or peeling off, rolling back and subduction of lower lithosphere while the upper lithosphere continues to be underplated or incorporated into the Himalayan thrust wedge removes a portion of the Indian plate with horizontal dimensions far greater than its thickness (Bird, 1978). Formation of Rayleigh–Taylor instabilities due to density anomalies such as eclogitization removes lower lithospheric material with a complicated planform of viscous blobs with lateral dimension of the order of, or less than, the vertical dimension (e.g. Conrad and Molnar, 1997). Our current study area covers too small an area of lithospheric foundering for us to confidently choose between delamination and de-blobbing, so here we focus on reporting observational results, though for convenience we use 'delamination' in the broadest sense possible to include all mechanisms for loss of the lower lithosphere.

Delamination of the Indian lower crust and roll-back of the Indian lithospheric mantle as suggested by our results helps to unravel the puzzle of accommodation of the post-collisional convergence between India and Asia. The post-collisional convergence is estimated to be ≥2000 km (Dupont-Nivet et al., 2010) but previous studies indicate that Indian lower crust has underthrust only ~150 km north of the YZS (Nábělek et al., 2009; Shi et al., 2015). The time required for this amount of underthrusting is less than 10 Ma based on an underthrusting rate of ~1.6 cm/yr (Wang et al., 2001), or about one fifth of the time elapsed since continental collision. Our results suggest that – at least in eastern Tibet – much of the convergence may have been accommodated by delamination of the Indian lower crust and the steep subduction of the Indian lithospheric mantle. Since the onset of India–Tibet collision, the delamination of the Indian lower crust and roll-back of the Indian mantle lithosphere has probably occurred more than once (DeCelles et al., 2002, 2011). High-wavespeed anomalies in the deep mantle beneath India observed tomographically (Li et al., 2008; Replumaz et al., 2010) can be explained as remnants of this process. The post-collisional ~26–10 Ma adakitic magmatism (Chung et al., 2005) and ~18–12 Ma intensive porphyry metallogenesis (Hou and Cook, 2009) observed in the southern Lhasa terrane may also be attributed to previous episodes of delamination of the Indian lower crust. A link between delamination and Miocene adakitic/ultrapotassic magmatism would further imply that delamination, like the magmatism, has occurred along the entire length of the Himalayan arc (Chung et al., 2005).

The north–south trending rifting is a marked phenomenon associated with the east–west extension in southern Tibet. Many models have been proposed to explain the rifting mechanism, such as gravitational collapse (England and Houseman, 1989), oblique convergence along an arcuate margin (McCaffery and Nábělek, 1998), delamination of mantle lithosphere beneath the rifts (Ren and Shen, 2008), or tearing of subducting Indian mantle lithosphere (Liang et al., 2012, 2016). Receiver-function and vertical deep-seismic-sounding profiling across the west flank of the YGR observed a 5-km step in the Moho consistent with down-to-the-east normal faulting and associated lower-crustal flow (Zhang et al., 2013; Tian et al., 2015). Our results presented here suggest that west–east extension of the Yadong–Gulu graben and the Cona–Sangri graben can be explained as resulting from delamination between, but perhaps not beneath, the grabens (cf. Tian et al., 2015), instead of the loss of lower-crustal material through eastward flow suggested by Zhang et al. (2013).

In summary, our closely spaced receiver-function profiles reveal dramatic west–east changes of the crustal and upper-mantle structure in the east-central India–Tibet collision zone. These results are consistent with a transition from underplating to steep subduction at ~91.5°E. Our results suggest that the vast convergence between the Indian and Eurasian continents may have been accommodated not only by underplating, but also by the delamination of the Indian lower crust and steep subduction of the Indian mantle lithosphere, consistent with modern estimates of a substantial mass deficit between original and modern crustal volumes in the orogen (e.g. Yakovlev and Clark, 2014).

## Acknowledgements

This research was funded by the Chinese Geological Survey (1212011220903, 1212011120185), the China National Natural Science Foundation (41374109), the U.S. National Science Foundation Continental Dynamics Program (EAR 9614616), the Deutsche Forschungsgemeinschaft and the Deutsches GeoForschungsZentrum – GFZ, Germany. Instruments for the INDEPTH III project were provided by the PASSCAL facility of the Incorporated Research Institutions for Seismology (IRIS) through the PASSCAL Instrument Center at New Mexico Tech and the Geophysical Instrument Pool of the Deutsches GeoForschungsZentrum – GFZ. We are grateful to two anonymous reviewers who provided many useful comments and suggestions that greatly improved the manuscript. The GMT

software package (Wessel and Smith, 1998) was used for production of most figures.

## Appendix A. Supplementary material

Supplementary material related to this article can be found online at http://dx.doi.org/10.1016/j.epsl.2016.07.051. These data include the Google map of the most important areas described in this article.

## References


Argand, E., 1924. La tectonique de l'Asie. Int. Geol. Congr. Rep. Sess. 13, 170–372.

Bird, P., 1978. Initiation of intracontinental subduction in the Himalaya. J. Geophys. Res. 83, 4975–4987.

Caldwell, W.B., Klemperer, S.L., Lawrence, J.F., Rai, S.S., 2013. Characterizing the Main Himalayan Thrust in the Garhwal Himalaya, India with receiver function CCP stacking. Earth Planet. Sci. Lett. 367, 15–27. http://dx.doi.org/10.1016/j.epsl.2013.02.009.

Chung, S.L., Chu, M.F., Zhang, Y., Xie, Y., Lo, C.H., Lee, T.Y., Lan, C.Y., Li, X.H., Zhang, Q., Wang, Y., 2005. Tibetan tectonic evolution inferred from spatial and temporal variations in post-collisional magmatism. Earth-Sci. Rev. 68, 173–196.

Conrad, C.P., Molnar, P., 1997. The growth of Rayleigh–Taylor-type instabilities in the lithosphere for various rheological and density structures. Geophys. J. Int. 129, 95–112.

DeCelles, P.G., Robinson, D.M., Zandt, G., 2002. Implications of shortening in the Himalayan fold-thrust belt for uplift of the Tibetan Plateau. Tectonics 21 (6). http://dx.doi.org/10.1029/2001TC001322, pp. 25.

DeCelles, P.G., Kapp, P., Quade, J., Gehrels, G.E., 2011. Oligocene–miocene kailas basin, southwestern Tibet: record of postcollisional upper-plate extension in the Indus-Yarlung suture zone. Geol. Soc. Am. Bull. 123 (7), 1337–1362.

Dupont-Nivet, G., Lippert, P.C., Van Hinsbergen, D.J., Meijers, M.J., Kapp, P., 2010. Palaeolatitude and age of the Indo–Asia collision: palaeomagnetic constraints. Geophys. J. Int. 182, 1189–1198.

England, P., Houseman, G., 1989. Extension during continental convergence, with application to the Tibetan Plateau. J. Geophys. Res. 94, 17561–17579.

Gao, R., Lu, Z., Klemperer, S.L., Wang, H., Dong, S., Li, W., Li, H., 2016. Crustal-scale duplexing beneath the Yarlung Zangbo suture in the western Himalaya. Nat. Geosci. 9, 555–560. http://dx.doi.org/10.1038/ngeo2730.

Hetényi, G., Cattin, R., Brunet, F., Bollinger, L., Vergne, J., Nábělek, J.L., Diament, M., 2007. Density distribution of the India plate beneath the Tibetan Plateau: geophysical and petrological constraints on the kinetics of lower-crustal eclogitization. Earth Planet. Sci. Lett. 264, 226–244.

Hou, Z., Cook, N.J., 2009. Metallogenesis of the Tibetan collisional orogen: a review and introduction to the special issue. Ore Geol. Rev. 36, 2–24.

Kind, R., Yuan, X., Saul, J., Nelson, D., Sobolev, S.V., Mechie, J., Zhao, W., Kosarev, G., Ni, J., Achauer, U., Jiang, M., 2002. Seismic images of crust and upper mantle beneath Tibet: evidence for Eurasian plate subduction. Science 298, 1219–1221. http://dx.doi.org/10.1126/science.1078115.

Kosarev, G., Kind, R., Sobolev, S.V., Yuan, X., Hanka, W., Oreshin, S., 1999. Seismic evidence for a detached Indian lithospheric mantle beneath Tibet. Science 283, 1306–1309. http://dx.doi.org/10.1126/science.283.5406.1306.

Le Roux-Mallouf, R., Godard, V., Cattin, R., Ferry, M., Gyeltshen, J., Ritz, J.F., Drupka, D., Guillou, V., Arnold, M., Aumaître, G., Bourlès, D.L., 2015. Evidence for a wide and gently dipping Main Himalayan Thrust in western Bhutan. Geophys. Res. Lett. 42, 3257–3265.

Leech, M.L., Singh, S., Jain, A.K., Klemperer, S.L., Manickavasagam, R.M., 2005. The onset of India–Asia continental collision: early, steep subduction required by the timing of UHP metamorphism in the western Himalaya. Earth Planet. Sci. Lett. 234, 83–97. http://dx.doi.org/10.1016/j.epsl.2005.02.038.

Li, C., Van der Hilst, R.D., Meltzer, A.S., Engdahl, E.R., 2008. Subduction of the Indian lithosphere beneath the Tibetan Plateau and Burma. Earth Planet. Sci. Lett. 274, 157–168. http://dx.doi.org/10.1016/j.epsl.2008.07.016.

Liang, X., Sandvol, E., Chen, Y.J., Hearn, T., Ni, J., Klemperer, S., Shen, Y., Tilmann, F., 2012. A complex Tibetan upper mantle: a fragmented Indian slab and no South-verging subduction of Eurasian lithosphere. Earth Planet. Sci. Lett. 333–334, 101–111. http://dx.doi.org/10.1016/j.epsl.2012.03.036.

Liang, X., Chen, Y., Tian, X., Chen, Y.J., Ni, J., Gallegos, A., Klemperer, S.L., Wang, M., Xu, T., Sun, C., Si, S., Lan, H., Teng, J., 2016. 3D imaging of subducting and fragmenting Indian continental lithosphere beneath southern and central Tibet using body-wave finite-frequency tomography. Earth Planet. Sci. Lett. 443, 162–175. http://dx.doi.org/10.1016/j.epsl.2016.03.029.

Ligorria, J., Ammon, C.J., 1999. Iterative deconvolution and receiver function estimation. Bull. Seismol. Soc. Am. 89, 1395–1400.

McCaffery, R., Nábělek, J., 1998. Role of oblique convergence in the active deformation of the Himalayas and southern Tibet Plateau. Geology 26, 691–694.

Nábělek, J., György, H., Vergne, J., Sapkota, S., Kafle, B., Jiang, M., Su, H., Chen, J., Huang, B.S., Hi-CLIMB Team, 2009. Underplating in the Himalaya–Tibet collision zone revealed by the Hi-CLIMB experiment. Science 325, 1371–1374. http://dx.doi.org/10.1126/science.1167719.

Powell, C.M., Conaghan, P.J., 1973. Plate tectonics and the Himalayas. Earth Planet. Sci. Lett. 20, 1–12.

Reading, A., Kennett, B., Sambridge, M., 2003. Improved inversion for seismic structure using transformed, S-wave vector receiver functions: removing the effect of the free surface. Geophys. Res. Lett. 30. http://dx.doi.org/10.1029/2003GL018090.

Ren, Y., Shen, Y., 2008. Finite frequency tomography in southeastern Tibet: evidence for the causal relationship between mantle lithosphere delamination and the North–South trending rifts. J. Geophys. Res. 113, B10316. http://dx.doi.org/10.1029/2008JB005615.

Replumaz, A., Negredo, A.M., Guillot, S., Villaseñor, A., 2010. Multiple episodes of continental subduction during India/Asia convergence: insight from seismic tomography and tectonic reconstruction. Tectonophysics 483 (1), 125–134.

Russo, R.M., 2012. Source-side shear-wave splitting and upper-mantle flow beneath the Arakan slab, India–Asia–Sundalind triple junction. Geosphere 8 (1), 21. http://dx.doi.org/10.1130/GES00534.1.

Schulte-Pelkum, V., Monsalve, G., Sheehan, A., Pandey, M.R., Sapkota, S., Bilham, R., Wu, F., 2005. Imaging the Indian subcontinent beneath the Himalaya. Nature 435, 1222–1225. http://dx.doi.org/10.1038/nature03678.

Shi, D., Zhao, W., Brown, L., Nelson, D., Zhao, X., Kind, R., Ni, J., Xiong, J., Mechie, J., Guo, J., Klemperer, S., Hearn, T., 2004. Detection of southward intracontinental subduction of Tibetan lithosphere along the Bangong-Nujiang suture by P-to-S converted waves. Geology 32, 209–212.

Shi, D., Wu, Z., Klemperer, S.L., Zhao, W., Xue, G., Su, H., 2015. Receiver function imaging of crustal suture, steep subduction, and mantle wedge in the eastern India–Tibet continental collision zone. Earth Planet. Sci. Lett. 414, 6–15.

Tapponnier, P., Xu, Z., Roger, F., Meyer, B., Arnaud, N., Wittlinger, G., Yang, J., 2001. Oblique stepwise rise and growth of the Tibet Plateau. Science 294, 1671–1677.

Taylor, M.H., Yin, A., 2009. Active faulting on the Tibetan Plateau and sounding regions relationships to earthquakes, contemporary strain, and late Cenozoic volcanism. Geosphere 5, 199–214.

Tian, X., Chen, Y., Tseng, T.L., Klemperer, S.L., Thybo, H., Liu, Z., Xu, T., Liang, X., Bai, Z., Zhang, X., Si, S., 2015. Weakly coupled lithospheric extension in southern Tibet. Earth Planet. Sci. Lett. 430, 171–177.

Tilmann, F., Ni, J., INDEPTH III Seismic Team, 2003. Seismic imaging of the downwelling Indian lithosphere beneath central Tibet. Science 300, 1424–1427.

Wang, Q., Zhang, P.Z., Freymueller, J.T., Bilham, R., Larson, K.M., Lai, X.A., You, X.Z., Niu, Z.J., Wu, J.C., Li, Y.X., Liu, J.N., Yang, Z.Q., Chen, Q.Z., 2001. Present-day crustal deformation in China constrained by global positioning system measurements. Science 294, 574–577. http://dx.doi.org/10.1126/science.

Wessel, P., Smith, W.H.F., 1998. New, improved version of generic mapping tools released. Eos 79, 579.

Wittlinger, G., Farra, V., Hetényi, G., Vergne, J., Nábělek, J., 2009. Seismic velocities in southern Tibet lower crust: a receiver function approach for eclogite detection. Geophys. J. Int. 177, 1037–1049.

Yakovlev, P.V., Clark, M.K., 2014. Conservation and redistribution of crust during the Indo-Asian collision. Tectonics 33, 1016–1027. http://dx.doi.org/10.1002/2013TC003469.

Yin, A., Harrison, T.M., Ryerson, F.J., Wenji, C., Kidd, W.S.F., Copeland, P., 1994. Tertiary structural evolution of the Gangdese thrust system, southeastern Tibet. J. Geophys. Res. 99, 18175–18201.

Zhang, Z.J., Chen, Y., Yuan, X.H., Tian, X.B., Klemperer, S.L., Xu, T., Bai, Z.M., Zhang, H.S., Wu, J., Teng, J.W., 2013. Normal faulting from simple shear rifting in South Tibet, using evidence from passive seismic profiling across the Yadong–Gulu Rift. Tectonophysics 606, 178–186.

Zhang, L.Y., Ducea, M.N., Ding, L., Pullen, A., Kapp, P., Hoffman, D., 2014. Southern Tibetan Oligocene–Miocene adakites: a record of Indian slab tearing. Lithos 210, 209–223.

Zhao, W., Kumar, P., Mechie, J., Kind, R., Meissner, R., Wu, Z., Shi, D., Su, H., Xue, G., Karplus, M., Tilmann, F., 2011. Tibetan plate overriding the Asian plate in central and northern Tibet. Nat. Geosci. 4, 870–873. http://dx.doi.org/10.1038/NGEO1309.

Zhao, W., Nelson, K.D., Project INDEPTH team, 1993. Deep seismic reflection evidence for continental underthrusting beneath southern Tibet. Nature 366, 557–559. http://dx.doi.org/10.1038/366557a0.

Zurek, B., 2008. The evolution and modification of continental lithosphere, dynamics of 'indentor corners' and imaging the lithosphere across the eastern syntaxis of Tibet. Ph.D. thesis. Lehigh University. viii+250.